Theoretical and Experimental Study of the Product Branching in the Reaction of Acetic Acid with OH Radicals

F. De Smedt, X. V. Bui, T. L. Nguyen, J. Peeters, and L. Vereecken*

Department of Chemistry, University of Leuven, Celestijnenlaan 200F, 3001 Leuven, Belgium

Received: November 22, 2004; In Final Form: January 11, 2005

The product distribution of the reaction of acetic acid, CH_3COOH, with hydroxyl radicals, OH, was studied experimentally and theoretically. Mass-spectrometric measurements at 290 K and 2 Torr of He of the CO_2 yield versus the loss of acetic acid yielded a branching fraction of 64 ± 14% for the abstraction of the acidic hydrogen as follows: $CH_3COOH + OH \rightarrow CH_3COO + H_2O \rightarrow CH_3 + CO_2 + H_2O$. A quantum chemical and theoretical kinetic analysis showed that the abstraction of the acidic hydrogen is enhanced relative to the abstraction of $-CH_3$ hydrogens because of the formation of a strong pre-reactive H-bonded complex, where the H-bonds are retained in the H-abstraction transition state. The potential energy surface of the reaction is explored in detail, and the reaction products of the individual channels are identified. The theoretical product branching is found to be critically dependent on the energetic and rovibrational differences between the H-abstraction transition states.

Introduction

For the HO_x budget in the atmosphere, oxygenated volatile organic compounds (VOCs) are important species, even when present only in trace concentrations. Among the oxygenates, acetic acid (CH_3COOH) has recently been recognized as an important species in the troposphere. The primary sources of acetic acid in the atmosphere are the reaction of peroxy acetyl radicals ($CH_3C(O)OO^\bullet$) with HO_2 and CH_3O_2[1] and direct emission from biomass burning.[2] The latter process is thought to make an important contribution to the high concentration (up to 2 ppbv) of acetic acid observed in the tropical upper troposphere,[3] even accounting for dissolution of acetic acid into rain. Very recently, at the low temperatures of the tropical tropopause, the fast equilibrium $HO_2 + (CH_3)_2CO \leftrightarrow (CH_3)_2C(OH)OO^\bullet$ followed by reaction with NO and then the subsequent fast decomposition $(CH_3)_2C(OH)O^\bullet \rightarrow CH_3 + CH_3COOH$ has been proposed[4] as an additional source of acetic acid. In view of the reported levels of acetic acid concentrations, CH_3COOH can be assumed to be a non-negligible source of methyl peroxy radicals,[3] thereby influencing the oxidative capacity of the upper troposphere.

The sources and sinks of acetic acid are not fully understood and quantified; thus there are inconsistencies in current atmospheric models. It is believed that the major acetic acid sink in the free and upper troposphere is the gas-phase reaction with the OH radical. So far, only a few studies have been performed on this particular reaction. The reaction can proceed through two reaction channels, both of which are H-abstractions; one channel leads to CH_3 and CO_2 and the other channel to $^\bullet CH_2COOH$. Like the reaction of OH with ketones and aldehydes,[5−10] addition on the carbonyl double bond (C═O) does not contribute significantly.

* Corresponding author. Email address: luc.vereecken@chem.kuleuven.ac.be.

$$CH_3COOH + {}^\bullet OH \rightarrow CH_3C(O)O^\bullet + H_2O \rightarrow CO_2 + {}^\bullet CH_3 + H_2O \quad (1a)$$

$$\rightarrow {}^\bullet CH_2COOH + H_2O \quad (1b)$$

The $CH_3C(O)O^\bullet$ radical will decompose rapidly into $^\bullet CH_3 + CO_2$ with a barrier of only some 5 kcal mol^{-1};[11] this process should occur on a nanosecond-to-microsecond time scale in all atmospheric conditions. The subsequent atmospheric oxidation of the radicals will always lead to $CH_2O + CO_2$ as the final products, in atmospheric conditions with sufficiently high levels of NO; this was confirmed experimentally.[12] The $^\bullet CH_3$ radicals will, as usual, be converted to CH_2O, and the $^\bullet CH_2COOH$ radical will react with O_2 and NO to form a β-substituted alkoxyradical ($^\bullet OCH_2COOH$). The dissociation of this radical, forming CH_2O and HOCO, is expected to have a barrier of about 3 kcal mol^{-1} [11]; HOCO, in turn, will oxidize to CO_2.[13] In less oxidative conditions with lower NO concentrations, the chemistry will shift to peroxy radical reactions and (hydro)peroxides may be formed. Even if the final products are the same for both channels, the existence of two initial reaction channels affects the overall rate coefficient of the $CH_3COOH + OH$ reaction and its temperature and pressure dependence. For other acids, the final atmospheric degradation products of the different initial reaction channels might be nonidentical.

Experimental data on the temperature dependence of the rate coefficient of the title reaction are scarce and sometimes contradictory: both negative[14,15] and positive[16] temperature dependencies are observed between 229 and 446 K. The current recommended value at 298 K is 8×10^{-13} cm^3 $molecule^{-1}$ s^{-1},[17,18] while the most recent experimental study by Butkovskaya et al.[15] on the overall rate constant between 229 and 300 K at 200 Torr of N_2 showed an overall rate constant at 298 K of 6.6×10^{-13} cm^3 $molecule^{-1}$ s^{-1} and a pronounced negative temperature dependence in good agreement with earlier results by Singleton et al.[14] Some information on the branching fraction

10.1021/jp044679v CCC: $30.25
Published on Web 02/15/2005

k_{1a}/k_1 and the reaction mechanism is also available. On the basis of isotope effects and the significantly lower reactivity of the dimer, Singleton et al.[14] concluded that abstraction of the acidic hydrogen is the dominant channel; their observations agree[14,19] with a two-channel mechanism involving hydrogen-bonded complexes and H-abstraction enhanced by tunneling through a potential energy barrier. The direct product measurements for reaction channel 1a by Butkovskaya et al.[15] yielded a branching fraction k_{1a}/k_1 of 64 ± 17% for T = 229−300 K and 200 Torr of N_2, based on the observed yield of CO_2 as a primary reaction product.

In this work, the branching fraction for the reaction of acetic acid with OH was determined experimentally at 290 K and 2 Torr of He by measuring the CO_2 yield from reaction 1a. In addition, a complementary theoretical investigation of the $CH_3COOH + OH$ reaction was performed; it supports the experimental product data, clarifies the intricate molecular mechanisms of this complex process, and reveals the crucial role of the various intermediate hydrogen-bonded complexes involved.

Experimental Study

Experimental Setup and Conditions. A multistage fast-flow reactor coupled to a molecular beam sampling mass spectrometry (MBMS) apparatus was used in this study. The fused-silica reactor consists of a cylindrical tube (internal radius R of 1.35 cm) equipped with a microwave sidearm and a set of two independently movable coaxial central injector tubes. The experimental setup and the cleaning procedure with final HF-passivation in order to suppress radical losses on the reactor walls have been described before.[20] The gas at the reactor exit is sampled through a 0.3 mm pinhole in the tip of a quartz cone, which gives access to three differentially pumped vacuum chambers. The resulting molecular beam is mechanically modulated by means of a chopper to allow phase-sensitive detection, and then it enters the last chamber which houses an axial electron-impact ionizer and a high-sensitivity Extranuclear quadrupole mass spectrometer. A lock-in amplifier separates the beam signal from the background signal.

Hydroxyl radicals are generated via the reaction $H + NO_2 \rightarrow NO + OH$. Hydrogen atoms are formed upstream in a 75 W microwave discharge through a H_2/He mixture and are reacted with NO_2 added through the outer central tube. The H-atoms are always in (slight) excess over NO_2. Acetic acid is fed into the reactor through the inner central tube. He was used as the carrier gas in all cases. Gases and liquids were used without further purification. He (99.9996%, Air Products) was used as the carrier gas for the discharge sidearm of the reactor, and He (99.995%, Indugas) was the main carrier gas for the inner and outer central tubes. The other gases were H_2 (5.0% in UHP He, Air Liquide), CO_2 (99.97%, Messer), and NO_2 (2.5% in UHP He, Air Products). Acetic acid (liquid) was of pro analysi quality (100%, Merck).

Methodology. To determine the relative importance of the two reaction channels for $CH_3COOH + OH$, we quantitatively measured one of the primary reaction products formed, namely, CO_2, for various initial concentrations of acetic acid and OH. The branching fraction of channel 1a, k_{1a}/k_1, can be determined directly from the measured CO_2-product concentration and the decrease in acetic acid concentration from the reaction with OH. Because of the multiple secondary reactions involving OH, one cannot use the decrease in the concentration of this species to determine the branching fraction. CO_2 production and CH_3COOH consumption were confirmed to be valid sensors for k_{1a}/k_1 through kinetic modeling with the Facsimile software,[21] as detailed below.

Absolute concentrations of NO_2 as the titrant gas and CO_2 as the calibrant gas were derived from the measured flows (regulated by flow controllers) of certified high-purity gas mixtures and the total pressure in the reactor. The initial concentration of hydroxyl radicals, $[OH]_0$, resulting from the reaction of NO_2 with an excess of H atoms, was taken to be equal to the added $[NO_2]_{add}$, neglecting OH-losses because of the OH self-reaction and OH + H recombination on the reactor walls. Note that $[OH]_0$ is not a critical quantity in this determination of k_{1a}/k_1. The $[OH]_0$ values in these experiments were in the range of 5×10^{12} to 5×10^{13} molecules cm^{-3}. CO_2 was measured at an ionizing-electron energy $E_{el} = 25$ eV. The CO_2^+ mass spectrometric signals were duly corrected, by blanc measurements, for a small $m/e = 44$ background contribution from trace CO_2 in the gas mixtures and found to be independent of added CH_3COOH. The detection limit of CO_2, defined as the standard deviation on the intercept of the calibration curve divided by the sensitivity, was around 3.0×10^{11} molecules cm^{-3} of CO_2.

The gas-phase concentration of the CH_3COOH reactant was obtained through a different procedure. A small He gas flow was bubbled through liquid acetic acid in a glass container thermostated at 290 K; He was introduced through a diffuser plate so that small gas bubbles were formed to ensure a high mass transfer of acetic acid into the gas phase. Typically, flows of 200−1200 sccm of He were used. The flow of He through the liquid CH_3COOH was kept constant by using a flow controller to ensure a constant concentration of acetic acid throughout each experiment, as confirmed by the constant mass spectrometric CH_3COOH signals ($m/e = 60$ and $E_{el} = 25$ eV). To calculate the gas-phase concentration, the weight loss of CH_3COOH over a period of several hours was measured at a constant bubbling He flow, as used in the pertinent experiments. Stable concentrations of CH_3COOH between 10^{13} and 10^{14} molecules cm^{-3} were easily obtained. Using the mass spectrometric signal $i_{CH_3COOH^+}$ and the absolute concentration $[CH_3COOH]_s$ calculated from the mass loss per unit time, we can derive the sensitivity of acetic acid as $S_{CH_3COOH} = i_{CH_3COOH^+}/[CH_3COOH]_s$. It must be noted that the dimerization of acetic acid in the gas phase is of no significance under the conditions of this study, given the low $[CH_3COOH]$ values. A similar procedure for the calibration of acetic acid has been used before[22] in studies of the reactions of ketones with OH.

Results. The branching fraction, k_{1a}/k_1, of the CO_2-forming channel was determined from the concentration of the CO_2 formed ($[CO_2]_{formed}$) and the decrease in the concentration of acetic acid ($[CH_3COOH]_{react}$) upon reaction with OH

$$k_{1a}/k_1 = [CO_2]_{formed}/[CH_3COOH]_{react}$$

The reaction conditions were changed by varying the initial concentrations of both the reactants. The initial $[CH_3COOH]_0$ was varied between 2.5×10^{13} and 1×10^{14} molecules cm^{-3}, and for each $[CH_3COOH]_0$, the initial $[OH]_0$ was changed in a range of 5×10^{12} to 5×10^{13} molecules cm^{-3}. All experiments were performed at 290 K and 2 Torr of total pressure (He is main bath gas), and the reaction time between the reactants, OH and CH_3COOH, was kept constant at ~6 ms. The results are summarized in Table 1. Because of the sometimes rather small decrease in the signal of acetic acid when reacting with OH, the spread of the individual branching fraction results is sometimes rather large. By averaging over all experiments, we determined the branching fraction of reaction 1a to be 64% with a standard deviation of 14%. Our experimental value of 64 ± 14% for the branching fraction of the CO_2-reaction channel is

TABLE 1: Experimental Determination of the Branching Fraction k_{1a}/k_1 of the CO_2-Forming Reaction Channel at 290 K and 2 Torr[a]

$[CH_3COOH]_0$ (molecules cm^{-3})	$[OH]_0$ (molecules cm^{-3})	branching fraction of channel 1a (%)	$[CH_3COOH]_0$ (molecules cm^{-3})	$[OH]_0$ (molecules cm^{-3})	branching fraction of channel 1a (%)
1.04×10^{14}	7.39×10^{12}	72	7.26×10^{13}	4.93×10^{12}	52
1.04×10^{14}	1.23×10^{13}	77	7.26×10^{13}	9.86×10^{12}	68
1.04×10^{14}	1.85×10^{13}	64	7.26×10^{13}	1.48×10^{13}	74
1.04×10^{14}	2.46×10^{12}	78	7.26×10^{13}	1.85×10^{13}	45
1.04×10^{14}	7.39×10^{12}	66	7.26×10^{13}	4.93×10^{12}	54
1.04×10^{14}	1.23×10^{13}	68	7.26×10^{13}	9.86×10^{12}	97
1.04×10^{14}	1.85×10^{13}	59	7.26×10^{13}	1.48×10^{13}	81
2.55×10^{13}	4.92×10^{12}	56	7.26×10^{13}	1.85×10^{13}	53
2.55×10^{13}	9.84×10^{12}	52	5.06×10^{13}	4.93×10^{12}	71
2.55×10^{13}	1.23×10^{13}	48	5.06×10^{13}	9.86×10^{12}	65
4.72×10^{13}	9.86×10^{12}	70	5.06×10^{13}	1.48×10^{13}	69
4.72×10^{13}	1.48×10^{13}	62	5.06×10^{13}	1.85×10^{13}	71
4.72×10^{13}	1.85×10^{13}	73	4.66×10^{13}	4.93×10^{12}	79
8.37×10^{13}	4.93×10^{12}	82	4.66×10^{13}	9.86×10^{12}	65
8.37×10^{13}	9.86×10^{12}	73	4.66×10^{13}	1.48×10^{13}	65
8.37×10^{13}	1.48×10^{13}	65	4.66×10^{13}	1.85×10^{13}	56
8.37×10^{13}	1.85×10^{13}	71	7.93×10^{13}	4.93×10^{12}	58
6.19×10^{13}	4.93×10^{12}	29	7.93×10^{13}	9.86×10^{12}	62
6.19×10^{13}	4.93×10^{12}	34	7.93×10^{13}	1.48×10^{13}	48
6.19×10^{13}	9.86×10^{12}	91	7.93×10^{13}	1.85×10^{13}	63
6.19×10^{13}	9.86×10^{12}	91	3.02×10^{13}	4.93×10^{12}	76
6.19×10^{13}	1.48×10^{13}	48	3.02×10^{13}	9.86×10^{12}	71
6.19×10^{13}	1.48×10^{13}	54	3.02×10^{13}	1.48×10^{13}	67
6.19×10^{13}	1.85×10^{13}	58	3.02×10^{13}	1.85×10^{13}	69
6.19×10^{13}	1.85×10^{13}	58	4.31×10^{13}	4.93×10^{12}	90
9.07×10^{13}	4.93×10^{12}	79	4.31×10^{13}	9.86×10^{12}	50
9.07×10^{13}	9.86×10^{12}	46	4.31×10^{13}	1.48×10^{13}	51
9.07×10^{13}	1.48×10^{13}	38	4.31×10^{13}	1.85×10^{13}	66
9.07×10^{13}	1.85×10^{13}	74			

[a] The reaction time was 6 ms.

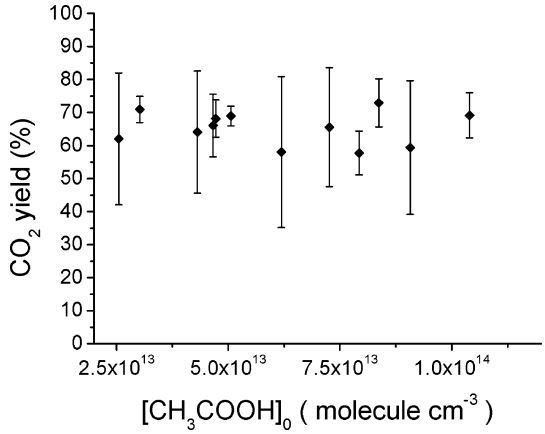

Figure 1. Branching fraction k_{1a}/k_1 for the reaction between OH and acetic acid at 290 K and 2 Torr as a function of the initial concentration of acetic acid, $[CH_3COOH]_0$. At a given $[CH_3COOH]_0$, the initial $[OH]_0$ ranged from 2×10^{12} to 2×10^{13} molecules cm^{-3}; the plot shows the average (symbol) with standard deviation (error bar) of the branching fraction measurements over this $[OH]_0$ range.

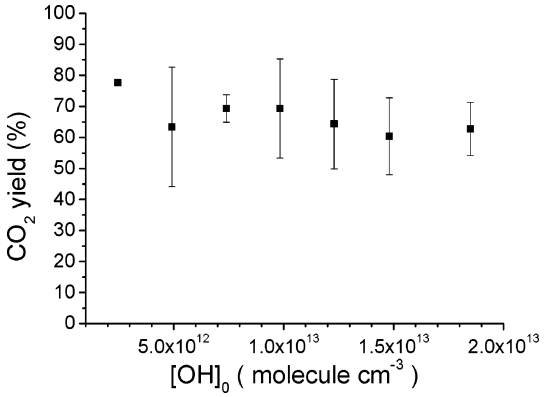

Figure 2. Branching fraction k_{1a}/k_1 of the reaction between OH and acetic acid at 290 K and 2 Torr as a function of the initial OH concentration, $[OH]_0$. At a given $[OH]_0$, the initial $[CH_3COOH]_0$ ranged from 2.5×10^{13} to 1.1×10^{14} molecules cm^{-3}; the plot shows the average (symbol) with standard deviation (error bar) of the branching fraction measurements over this $[CH_3COOH]_0$ range.

nearly identical to the value reported very recently by Butkovskaya et al.,[15] 64 ± 17%.

To check for possible secondary reactions which could influence the determination of the branching fraction, the dependence of the branching fraction data on the initial acetic acid and the initial OH concentration was checked by sorting the branching fraction results as functions of the initial concentrations. These dependencies are depicted in Figures 1 and 2; no meaningful effect on the experimentally determined branching fraction can be discerned as a function of either the initial CH_3COOH concentration or the initial concentration of OH.

Kinetic Modeling. The acetic acid−OH reaction system was also investigated by means of kinetic modeling with the Facsimile software[21] using a kinetic model, with 26 reactions and 27 different species, that describes our experimental conditions accurately. The most important reactions in the model are given in Table 2. Given the low reactivity of the vinoxy-resonance stabilized $^{\bullet}CH_2COOH$ radical (inc. toward CH_3-COOH), the lack of easily accessible CO_2-forming reactions from this radical (in the absence of O_2/NO), and its low concentration, secondary reactions of $^{\bullet}CH_2COOH$ are unlikely to affect the CH_3COOH and CO_2 concentrations and need not be included in the model. The kinetic simulation was done with an overall rate constant[23] for the CH_3COOH + OH reaction of 7.8×10^{-13} cm^3 $molecule^{-1}$ s^{-1} and a branching fraction of

TABLE 2: Some Important Reactions in the Kinetic Model of the Reaction between OH and Acetic Acid at 298 K and 2 Torr of He

reaction	ref	k (cm^3 $molecule^{-1}$ s^{-1})
$CH_3COOH + OH \rightarrow CH_2COOH + H_2O$[a]	15,23	2.8×10^{-13}
$CH_3COOH + OH \rightarrow CH_3 + CO_2 + H_2O$[a]	15,23	5.0×10^{-13}
$CH_3 + OH \rightarrow CH_3OH$	24	6.0×10^{-12}
$CH_3 + OH \rightarrow {}^1CH_2 + H_2O$	24	5.2×10^{-11}
$CH_3 + CH_3 \rightarrow C_2H_6$	24	3.0×10^{-11}
${}^1CH_2 + H_2O \rightarrow CH_3 + OH$	24	1.2×10^{-10}
${}^1CH_2 + He \rightarrow {}^3CH_2 + He$	25	3.3×10^{-12}
${}^1CH_2 + CH_3COOH \rightarrow$ products	26	5.8×10^{-10}
${}^1CH_2 + H_2O \rightarrow {}^3CH_2 + H_2O$	24	6.0×10^{-12}
${}^3CH_2 + OH \rightarrow CH_2O + H$	27	3.0×10^{-11}
${}^3CH_2 + CH_3 \rightarrow C_2H_4 + H$	28	7.0×10^{-11}

[a] Overall rate constant $k_1 = 7.8 \times 10^{-13}$ cm^3 $molecule^{-1}$ s^{-1} [23] and branching $k_{1a} = 64\%$.[15]

64% for 1a, as obtained experimentally in this work and the work of Butkovskaya et al.[15] Various initial concentrations of acetic acid and OH were used. The concentration of the bath gas He was fixed at 5×10^{16} molecule cm^{-3}.

From these kinetic modeling calculations, we learned that the branching fraction value derived from $[CH_3COOH]_{react}$ and $[CO_2]_{formed}$ is only slightly influenced by secondary reactions, i.e., an underestimation between 2 and 3%. CO_2, a primary reaction product of reaction channel 1a, does not participate in important secondary reactions in our experimental conditions and, therefore, can be used reliably to determine the relative importance of channel 1a. The reaction responsible for the slight underestimation is the reaction between acetic acid and ${}^1CH_2$ (Table 2) with singlet CH_2 formed in the secondary reaction of OH with $^{\bullet}CH_3$ radicals. As the predicted underestimation is significantly less than the experimental error, this slight bias was neglected in this report.

An alternative approach deriving the branching fraction from $[CO_2]_{formed}$ relative to $[OH]_{reacted}$ would lead to a pronounced underestimation of the branching fraction, namely, an underestimation by a factor of 5 based on the reaction currently included in the model. This is a result of OH not only reacting with acetic acid but also being removed by fast secondary reactions, such as the reaction with $^{\bullet}CH_3$, a primary product. The reaction of $^{\bullet}CH_3$ with OH forms singlet CH_2 among other species which leads to further secondary removal of OH.

Theoretical Study

The $CH_3COOH + OH$ reaction can proceed via the following three mechanisms: (1) OH-addition to the carbon of the C=O group in acetic acid, (2) hydrogen abstraction from the methyl group, and (3) H-abstraction from the $-COOH$ group. The first channel, OH-addition to the carbonyl bond, is expected to be a minor channel: for both aldehydes[5−8] and ketones[9,10] significant barriers were found for this channel. As the methyl C−H bond strength (98 ± 2 kcal mol^{-1}) is weaker by about 12 kcal mol^{-1} when compared to that of the acidic O−H bond (110 ± 2 kcal mol^{-1}),[29,30] one expects the H-abstraction from the methyl group to be, by far, the dominant reaction channel. However, experimental evidence (e.g., refs 14 and 15 and this work) indicates that it is, in fact, the acidic H that is being abstracted for an important, even dominant, fraction. Hence, ab initio/DFT calculations and theoretical kinetic analyses are required to elucidate the mechanism of the $CH_3COOH + OH$ reaction.

All ab initio and DFT calculations described below were done employing the Gaussian-98 program.[31] The theoretical kinetic calculations involved both RRKM-ME analyses,[32−34] using the URESAM program,[35] and transition state theory (TST)[36−38] calculations, including tunneling corrections.[39]

Quantum Chemical Characterization. The stationary points, both mimima and transition states, on the potential energy surface (PES) of the $CH_3COOH + OH$ reaction were located using the B3LYP method[40,41] in combination with the 6-311++G-(2df,2pd) basis set. To improve the accuracy of the relative energies for quantitative predictions and kinetic analysis, a modified version of the G2M(CC,MP2) method[42] was used to calculate single point energies. In our modification, the original 6-311G(d,p) and 6-311+G(3df,2p) basis sets were replaced by the correlation-consistent aug-cc-pVDZ and aug-cc-pVTZ basis sets, respectively, which include diffuse orbitals to improve the description of long-range effects, such as hydrogen bonds. It is expected that the relative energies calculated with our modified G2M(CC,MP2) method approach those at the CCSD(T)/aug-cc-pVTZ level. The relative energies calculated at the various levels of theory from the B3LYP optimized geometries are listed in Table 3. The G2M energies were used to construct the PES, which is shown in Figure 3. As seen in Table 3, the B3LYP energies agree reasonably with CCSD(T) and G2M for most of the structures; the differences are about 1−5 kcal mol^{-1}. An important exception to this is **TS3**, which shows a large difference from about 8 kcal mol^{-1} at the B3LYP/6-311++G-(2df,2pd) level to about 13 kcal mol^{-1} at the B3LYP/6-31G-(d_{5d},p) level when compared to the results from CCSD(T) and G2M. The values at the CCSD(T) level of theory are in good agreement, within ~0.5 kcal mol^{-1}, with those of the G2M method; the single exception is a 2 kcal mol^{-1} difference for one set of products, $CH_3 + H_2CO_3$.

TS1, **TS2**, and **TS3** (Figure 3) are key transition states. They are the rate-determining transition states, and they control the product distribution. In view of the exceptional behavior of **TS3** in the preceding calculations, we further investigated these key transition states using both B3LYP-DFT and MP2 levels of theory with various basis sets. Their relative energies were then refined using the G2M(CC,MP2) method described above. The values calculated at the various levels of theory are summarized in Table 4.[43] In comparison with the values obtained from the CCSD(T) and G2M methods, the values from the B3LYP method underestimate the barrier height while those from the MP2 method overestimate it. The MP2 and B3LYP relative energies for the TS suffer from well-known defects, e.g., an underestimation of H-abstraction energy barriers for B3LYP-DFT. The CCSD(T) and G2M values on the respective MP2 and B3LYP geometries agree well with each other for **TS1** and **TS2**: the largest discrepancy is less than 0.5 kcal mol^{-1} indicating that the CCSD(T) and G2M methods work well for both optimized geometries; therefore, the relative energies do not depend strongly on the optimized geometries. However, a discrepancy up to 1.6 kcal mol^{-1} between the G2M//MP2 and G2M//B3LYP levels was found for **TS3**.

Finally, the G3 theory,[44] which is based on MP2/6-31G(d) geometries, was also applied. The relative energies at the G3 level of theory for **TS1**, **TS2**, and **TS3** are about 2 kcal mol^{-1} higher than those at the G2M(CC,MP2) level but reproduce the **TS1**/**TS2**/**TS3** near-isoergicity of the G2M//MP2 results. However, if we use the barrier heights computed with G3 theory, we derive absolute rate constants which are much too small when compared to those from the experimental data. The barrier heights calculated with the G2M(CC,MP2) method yield absolute rate constants in much better agreement with the experimental data.

TABLE 3: Calculated Relative Energies, ZPE-Corrected, for Stationary Points in the Reaction CH_3COOH + OH Using Various Levels of Theory

	relative energy (kcal mol^{-1})			
species	B3LYP/ 6-31G(d5d,p)	B3LYP/ 6-311++G(2df,2pd)	CCSD(T)/ aug-cc-pVDZ[a]	G2M[a]
$CH_3COOH + {}^{\bullet}OH$	0.0	0.0	0.0	0.0
$CH_3C(O)O^{\bullet} + H_2O$	−10.5	−12.1	−6.4	−6.7
$H_2C^{\bullet}COOH + H_2O$	−16.1	−20.3	−17.8	−18.5
$^{\bullet}CH_3 + H_2CO_3$	−18.3	−17.5	−13.8	−16.2
$^{\bullet}CH_3 + CO_2 + H_2O$	−19.6	−26.4	−21.8	−22.9
Com1	−7.2	−4.4	−5.1	−5.1
Com2	−4.5	−2.2	−3.1	−3.1
Com3	−11.6	−6.6	−7.3	−7.3
Com4	−14.3	−10.8	−5.5	−5.7
Com5	−15.2	−14.4	−10.6	−10.6
Com6	−22.7	−24.2	−23.1	−23.7
Com7	−20.7	−22.4	−21.3	−21.9
Com8	−3.0	1.7	−0.4	−0.8
TS1	−1.3	0.2	3.9	4.0
TS2	−1.3	−0.2	3.6	3.7
TS3	−11.3	−6.2	2.1	1.6
TS4	−4.8	−3.7	−4.1	−4.2
TS5	5.0	8.8	9.2	9.5
TS6	1.6	5.2	6.7	5.3
TS7	−5.1	−7.6	−3.8	−4.4
TS8	−10.6	−11.3	−6.7	−7.9

[a] Based on the unscaled ZPE and optimized geometry at the B3LYP/6-311++G(2df,2pd) level.

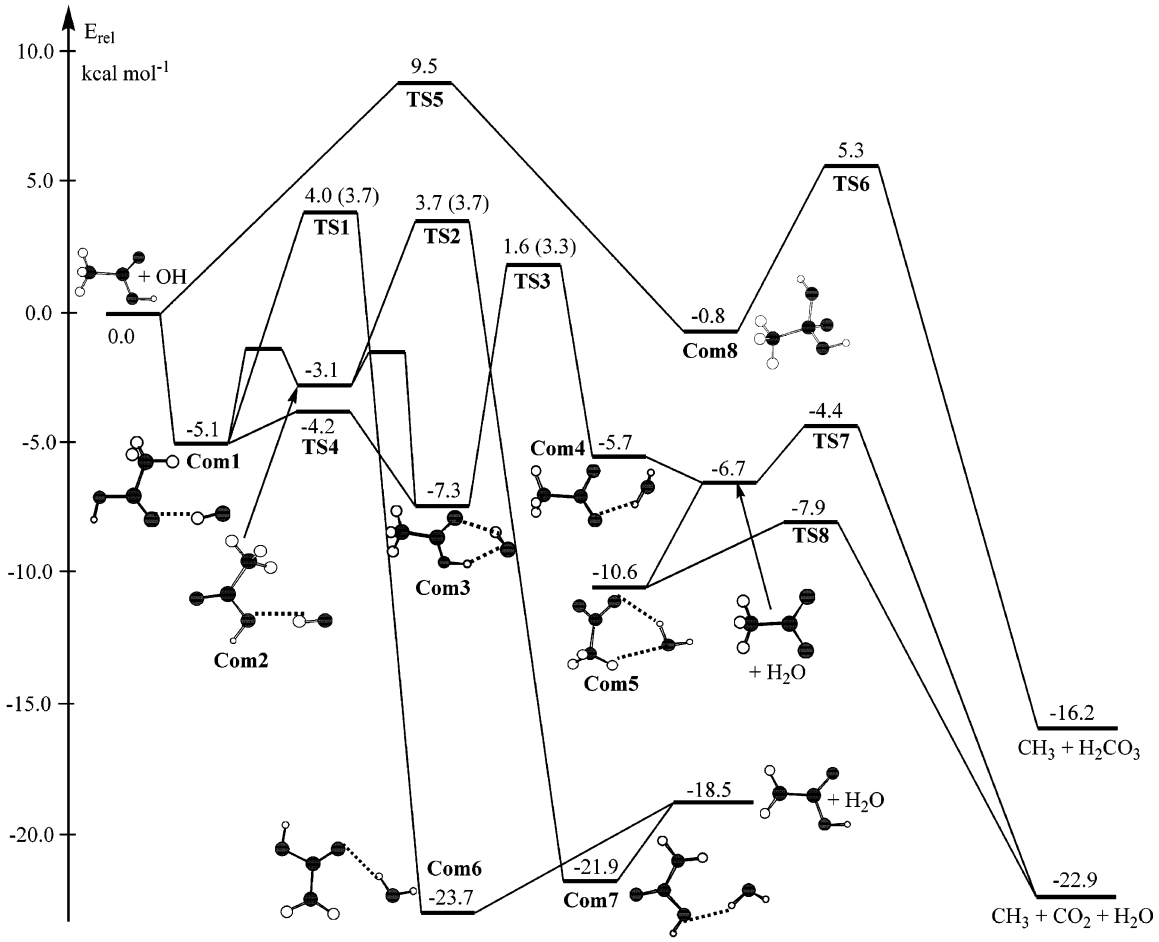

Figure 3. Potential energy surface for the OH + CH_3COOH reaction, constructed using the G2M(CC,MP2)//B3LYP/6-311++G(2df,2pd) level of theory. Values in parentheses were computed using G2M(CC,MP2)//MP2/6-311++G(2df,2pd).

Unless otherwise mentioned, the values of the relative energies used below for the discussions and kinetic analyses are those obtained at the G2M//B3LYP/6-311++G(2df,2pd) level of theory. For **TS1**, **TS2**, and **TS3**, we used an average of the values at the G2M//MP2 and G2M//B3LYP levels, i.e., barrier heights of 3.8, 3.7, and 2.4 kcal mol^{-1}, respectively, with a probable error of ±1 kcal mol^{-1} (1.5 kcal mol^{-1} for **TS3**).

TABLE 4: Calculated Relative Energies (in kcal mol^{-1}) of TS1, TS2, and TS3 Relative to the Reactants, CH_3COOH + OH, Using Various Levels of Theory

level of theory	TS1	TS2	TS3
B3LYP/6-31G(d5d,p)	−1.3	−1.3	−11.3
B3LYP/6-311++G(2df,2pd)	0.2	−0.2	−6.2
MP2/6-31G(d5d,p)	8.2	8.5	7.7
MP2/6-311++G(2d,2p)	6.7	6.9	9.3
CCSD(T)/aug-cc-pVDZ//B3LYP[a]	3.9	3.6	2.1
CCSD(T)/aug-cc-pVDZ//MP2[b]	3.7	3.6	3.8
G2M//B3LYP[a]	4.0	3.7	1.6
G2M//MP2[b]	3.6	3.6	3.2
G2M//MP2/6-31G(d5d,p)[c]	3.8	3.9	3.2
G2M//MP2/6-311++G(2df,2pd)	3.7	3.7	3.3
G3	5.3	5.2	5.3

[a] Using the unscaled ZPE and optimized geometry calculated at the B3LYP/6-311++G(2df,2pd) level. [b] Using the ZPE scaled by 0.9748 (ref 43) and optimized geometry calculated at the MP2/6-311++G(2d,2p) level. [c] Using the ZPE scaled by 0.9608 (ref 43) and optimized geometry calculated at the MP2/6-31G(d5d,p) level.

Discussion of the Reaction Mechanism. The three reaction mechanisms for the CH_3COOH + OH reaction are as follows: addition/fragmentation, H-abstraction from $-CH_3$, and H-abstraction from the OH group. The addition of OH on the carbon of the C═O group forms a $CH_3C(OH)_2O^\bullet$ radical intermediate, **Com8** (Figure 3), via **TS5** with a barrier height of 9.5 kcal mol^{-1}. **TS5** is the highest entrance transition state, about 5.5−7.0 kcal mol^{-1} higher than the abstraction transition states (**TS1**, **TS2**, and **TS3**). As a consequence, this channel is too slow to compete with the H-abstraction channels at atmospheric temperatures and will, therefore, not be important. Many internal rotameric forms exist for the addition product, each with different H-bonds and different relative energies. All rotameric forms of **Com8** can decompose to $CH_3 + H_2CO_3$ via **TS6** with barrier heights of about 6.1 kcal mol^{-1}.

The dominant channels in the CH_3COOH + OH reaction are the abstraction mechanisms. To access the actual abstraction transition states, the OH radical will first approach acetic acid to form H-bonded complexes of which we characterized several. Some of these complexes are energetically above the CH_3COOH + OH reactants (Figure 4) and are formed from the complexation of OH with the higher-energy non-H-bonded rotamer of acetic acid. H-Bond breaking in acetic acid faces a barrier of 11.6 kcal mol^{-1} [45] with the TS much higher in energy than those for both the addition and abstraction channels, and the non-H-bonded acetic acid rotamer lies about 5 kcal mol^{-1} above the most stable rotamer. Hence, these complexes are kinetically unimportant at atmospheric temperatures. Three energetically much more favorable H-bonded CH_3COOH- OH complexes are shown in Figure 3; **Com1**, **Com2**, and **Com3** are 5.1, 3.1, and 7.3 kcal mol^{-1} below the reactants, respectively, with **Com3** being the most stable because of its two hydrogen bonds. The CH_3COOH- OH complexes can interconvert comparatively easily, e.g., **Com1** isomerizes to **Com3** via **TS4** with a barrier height of only 0.9 kcal mol^{-1}; these rearrangement transition states lie below the energy level of the initial reactants and well below the transition states for chemical reaction. Hence, these complexes should establish a mutual equilibrium and an equilibrium with the noncomplexed reactants much faster than the chemical H-abstraction reactions take place, especially at the relevant atmospheric temperatures. Given that **Com3** is the most stable rotamer, it will contribute the most to the thermal equilibrium population and is, therefore, the key species in the initial complexation of OH with CH_3COOH. The initial complexation occurs through a long-range barrierless association, and a quantitative theoretical kinetic treatment of this association and the reverse dissociation would probably require trajectory dynamic calculations on an accurate PES. Such calculations are computationally prohibitively expensive and of little relevance to the scope of this paper given the expected fast equilibria as detailed above. Different H-abstraction channels are accessible depending on the position of the OH radical in the complex. According to TST, when the complexes are in thermal (quasi) equilibrium with each other and the reactants, the rates of reaction through these different channels should be controlled (quasi) uniquely by the energies and partition functions of the three transition states (**TS1**, **TS2**, and **TS3**) and of the initial reactants.

If one starts from the CH_3COOH- OH complexes **Com1** and **Com2**, a 1,5-H-shift via **TS1** and **TS2** with barrier heights of 8.9 and 6.8 kcal mol^{-1} (both about 4 kcal mol^{-1} above the reactants) leads to the $^\bullet CH_2COOH-$ H_2O complexes **Com6** and **Com7**. These chemically activated complexes dissociate readily to $^\bullet CH_2COOH + H_2O$.

A 1,5-H-shift in the most stable CH_3COOH- OH complex, **Com3**, via **TS3** with a barrier height of 9.7 kcal mol^{-1} (between 1.5 and 3.5 kcal mol^{-1} above the reactants) leads to **Com4**, a weakly bonded complex of H_2O and $CH_3C(O)O^\bullet$, which will dissociate spontaneously to the separated products H_2O + $CH_3C(O)O^\bullet$, especially since the complex inherits a large internal energy from the H-shift reaction. $CH_3C(O)O^\bullet$, in turn, is also chemically activated and dissociates easily to CH_3 + CO_2 with a barrier of only 2.3 kcal mol^{-1}, according to the present results. Earlier calculations confirmed this low barrier to dissociation, predicting a barrier of about 5 kcal mol^{-1}.[11] There are other complexes of H_2O with $CH_3C(O)O^\bullet$, such as **Com5** with two hydrogen bonds. This structure is 3.9 kcal mol^{-1} more stable than the separated products, $H_2O + CH_3C(O)O^\bullet$, but can only be formed directly through higher-energy pathways (Figure 4), making these complexes less important for room-temperature gas-phase kinetics. In an aqueous medium, such as aerosol particles, however, complexes such as **Com5** could be formed using H_2O from the solvent bulk and could affect the kinetics of the system somewhat even if the final products, $CH_3 + H_2O + CO_2$, remain the same after **Com5** fragmentation via **TS8** with a barrier height of 2.7 kcal mol^{-1}.

Kinetics of the Product Distribution. Despite the well-established fact that a carboxylic O−H bond is substantially stronger than a C−H bond, the results from both our experiment and Butkovskaya et al.[15] indicate that abstraction of the acidic hydrogen is faster than abstraction of the methyl hydrogens. The key feature of the potential energy surface enabling this result is the strong hydrogen bond between the OH-radical and the −COOH group in acetic acid, >7 kcal mol^{-1}, which remains intact and equally strong in the transition state for abstracting the acidic hydrogen. The geometries of the transition states for methyl H-abstraction on the other hand show much weaker, if any, H-bond interactions between the OH-radical and the acidic group, despite the existence of pre-reactive H-bonded complexes, since the OH-radical needs to reposition itself to create optimal orbital overlap with the methyl hydrogens to enable their abstraction. Hence, H-bonding in the acidic H-abstraction lowers this TS strongly, even to the point where the relative energies of methyl and acidic H-abstraction TSs become roughly comparable and even somewhat favor acidic H-abstraction. The RRKM-ME analyses for this reaction system indicate that this is a necessary condition to explain the experimentally observed product distribution supported, in turn, by the high-level quantum chemical G2M calculations. Further RRKM-ME

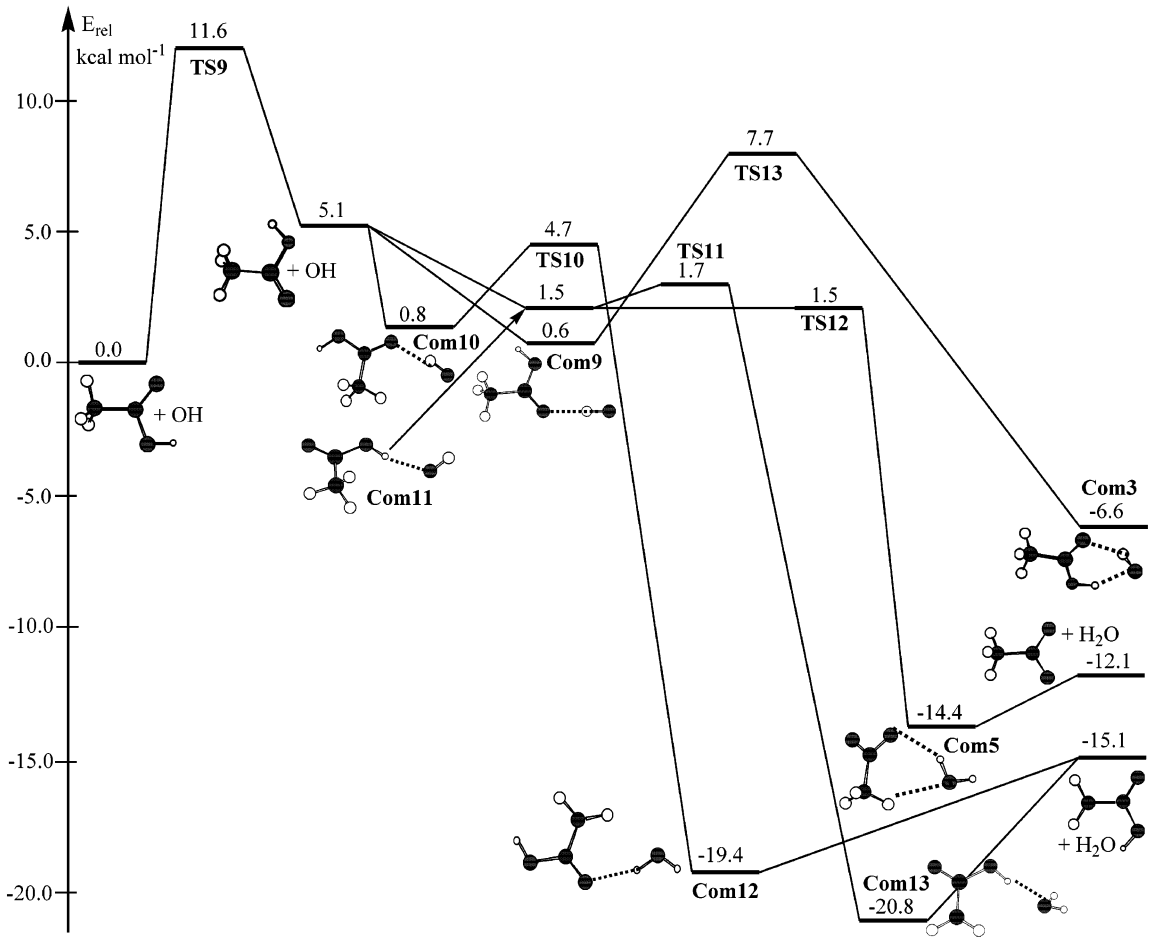

Figure 4. B3LYP/6-311++G(2df,2pd) potential energy surface for the reaction of OH with the high-energy rotamer of acetic acid.

branching ratio sensitivity analyses with respect to the relative energies of the two types of H-abstraction showed that the branching is critically dependent on the relative energies of **TS1** and **TS2** on one hand versus **TS3** on the other.

Unfortunately, while the highest levels of theory used in this work agree within a few tenths of a kilocalories per mole on the barrier heights of **TS1** and **TS2** for methyl H-abstraction, the relative energy of **TS3** for acidic H-abstraction is subject to a much larger uncertainty ($\sim$1.5 kcal mol^{-1}). The large uncertainty results in a wide margin of error for the RRKM-ME or TST predictions at room temperature; the predictions indicate that acidic H-abstraction is certainly competitive with methyl H-abstraction but that branching fractions of 10−90% and beyond can be obtained depending on the set of input parameters used. Since the uncertainty involves the lowest-lying transition state, there are also large errors on the predicted absolute rate coefficient for the CH_3COOH + OH reaction. As such, the quantum chemical data available at this time qualitatively support the experimental observations but are unable to quantitatively predict or support the branching ratio and absolute rate coefficients with a reasonable level of accuracy.

We attempted to obtain a better estimate for the relative energy of **TS3** by optimizing the theoretically predicted branching ratio, using TST, to match the experimental fraction of 64%; in this optimization, the relative energies of **TS1** and **TS2** were kept constant. On the basis of the B3LYP-DFT vibrational frequencies (used unscaled), an optimal fit for the **TS3** relative energy of 3.08 kcal mol^{-1} above the C_3HCOOH + OH reactants was obtained; the use of the MP2 wavenumbers (scaled by 0.9748)[43] and a relative energy of 1.68 kcal mol^{-1} yielded the best correspondence. This reverses the relative ordering of the G2M//MP2 versus G2M//B3LYP **TS3** energies, and the uncertainty of the relative energy remains about 1.4 kcal mol^{-1}. The lower barrier height for the optimization using MP2 frequencies is indicative of the more rigid **TS3** transition state characterized at this level of theory in comparison to that of B3LYP. Also, the B3LYP imaginary wavenumbers differ strongly between **TS1**/**TS2** ($\sim$700*i* cm^{-1}) and **TS3** ($\sim$1300*i* cm^{-1}), so that the inclusion of a tunneling correction, modeled using an asymmetric Eckart barrier,[39] alters the predicted ratio by a factor of $\sim$3.5. In contrast, the MP2 imaginary wavenumbers are much higher but closer together (all within 1900*i*−2200*i* cm^{-1}) so that the inclusion of tunneling hardly affects the relative contributions. The predicted temperature dependence of the branching, calculated after tuning the 290 K branching to 64% by adjusting the **TS3** barrier height, also differs between the two sets of vibrational data: the B3LYP vibrational characteristics lead to a steeper *T*-dependence (32% at 400 K, 82% at 250 K, and 96% at 210 K), while the MP2 data have a less pronounced temperature dependence (48% at 400 K, 70% at 250 K, and 76% at 210 K). Note that both methods agree that the contribution of acidic H-abstraction increases with lower temperature. The data from Butkovskaya et al.[15] seem to suggest a very slightly decreasing contribution (4% decrease from 298 to 250 K), although this change is dwarfed by the experimental error (about 17% absolute) and, therefore, might be an artifact. Using the *relative* energies for **TS1**, **TS2**, and **TS3** obtained by fitting the product distribution as detailed above, we attempted to optimize the *absolute* barrier heights by optimizing the [**TS1**,**TS2**,**TS3**] set of barrier heights simultaneously so that the

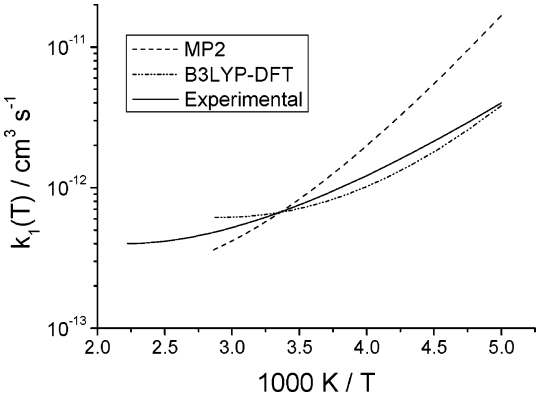

Figure 5. Arrhenius plot of the total rate coefficients k_1(T). The reference line is the modified Arrhenius expression[15] obtained from experimental data by Butkovskaya et al.[15] and Singleton et al.[14] The theoretical results were obtained by adjusting the barrier heights for **TS1**, **TS2**, and **TS3** so that TST calculations on the product distribution and absolute rate coefficient, using the rovibrational data from B3LYP-DFT and MP2 calculations, match the experimental data.

TST-predicted total absolute rate coefficient at 298 K matches the experimentally observed rate coefficient, k_1 (298 K), of 6.6 $\times$ 10^{-13} cm^3 molecule^{-1} s^{-1}.[14,15] The adjusted barrier heights obtained in this two-step procedure yield TST rates that match both the experimental total rate coefficient and the experimental product distribution at 298 K. Using the B3LYP-DFT rovibrational data, we found an optimal correspondence for barrier heights of 1.20, 0.90, and 0.28 kcal mol^{-1} for **TS1**, **TS2**, and **TS3**, respectively; for the MP2 set of rovibrational data, we obtained barrier heights of 3.28, 3.28, and 1.27 kcal mol^{-1}, respectively. The overall rate coefficients obtained at both levels of theory are shown in Figure 5 and compared to the experimental data. Both curves show a negative temperature dependence, in agreement with the experimental data. The temperature dependence using MP2 wavenumbers is significantly steeper than that of the experimental data which might suggest that the high imaginary wavenumbers obtained at the MP2 level of theory result in an overcorrection for tunneling. The B3LYP-based rate coefficient matches the experimental curve better at lower *T*, but its curvature is a bit too pronounced so that the high-temperature data are overestimated some. For both sets of rovibrational data, the optimization of the barrier heights to fit the experimental data required significant changes from the native energies or single point G2M energies, both absolute and relative.

Our theoretical treatment of the temperature dependence of the branching ratio and absolute rate coefficient is far from complete and should include, among other things, a more detailed treatment of the tunneling effects and the impact of the $-CH_3$ internal rotor. Earlier theoretical work on the acetone + OH reaction[10] already showed that tunneling from pre-reactive complexes has an important effect on the relative importance of different reaction channels. However, a more detailed theoretical kinetic analysis has little predictive value until the uncertainties on the H-abstraction characteristics, in particular **TS3**, are resolved. The G2M energies prior to ZPE correction are identical for the reactants for both methods but differ by 0.92 kcal mol^{-1} for **TS3**. This indicates that MP2 and B3LYP disagree on the geometry of this transition state. Furthermore, the ZPE correction from reactants to **TS3** also differs by 0.58 kcal mol^{-1}, further escalating the energy difference, and is indicative of a difference in TS rigidity between the two levels of theory. The difference in rigidity can also be seen from the difference in barrier height upon matching the predicted product distribution to the observed branching (see above). In addition, the disagreement in frequency analysis between MP2 and B3LYP is borne out by the large differences in imaginary wavenumbers, affecting both the absolute and relative tunneling corrections. At present, it seems that neither the MP2/6-311++G(2d,2p)- nor B3LYP/6-311++G(2df,2pd)-based data are of sufficient accuracy to fully conform to the experimental data. Such discrepancies can only be resolved by higher-level geometry optimizations and frequency analysis, which is computationally very expensive. We will address these issues in later theoretical work.

The potential energy surface available here is sufficiently accurate to predict the nature of the products finally formed for each of the entrance channels. Also, it shows that abstraction of the acidic hydrogen is energetically feasible and competitive with abstraction of the methyl hydrogens despite the difference in bond strength. The relative energies of the key transition states **TS1**, **TS2**, and **TS3** are characterized within 1.5 kcal mol^{-1}, but as both the absolute and the relative rates of reaction through these transition states are too sensitive to the exact value, a definitive quantitative prediction of the temperature-dependent overall rate coefficient and branching ratio is not possible as yet.

Conclusions

An experimental study of the branching ratio of the CH_3-COOH + OH reaction at 290 K and 2 Torr of He showed a branching ratio of 64 $\pm$ 14% for the abstraction of the acidic hydrogen based on the amount of CO_2 formation by that product channel compared to the amount of acetic acid consumed. This result is in excellent agreement with recent experimental work by Butkovskaya et al.[15] Quantum chemical calculations on the potential energy surface of the title reaction show that its kinetics and product distribution, in particular the acidic H-abstraction, are greatly enhanced and largely controlled by the formation of very stable H-bonded pre-reaction complexes. From these H-bonded complexes, the reaction proceeds by H-abstraction reactions where abstraction of the acidic hydrogen is competitive with abstraction of the methyl hydrogen despite the large difference in bond strength. The addition of OH onto the carbonyl double bond is predicted to be negligible at room temperature. The products formed in each of the reaction channels are characterized. Theoretical prediction of the temperature-dependent absolute rate coefficient and product branching is critically sensitive to the characteristics of the acidic H-abstraction transition state, **TS3**, and will be examined in more detail in a follow-up study.

Acknowledgment. This work was carried out in part in the frame of the Belgian research program on Global Change and Sustainable Development, funded by the Federal Office for Scientific, Technical and Cultural Affairs, and of the FP5 program of the European Commission (Environment, project Utopihan-Act). The authors are also indebted to the Fund for Scientific Research−Flanders (postdoctoral mandate and research project) and to the KULeuven Research Council (OT and GOA).

Supporting Information Available: Geometries, energies and vibrational wavenumbers of all of the structures discussed in this text or displayed in the figures at the B3LYP and MP2 levels of theory. This information is available free of charge via the Internet at http://pubs.acs.org.

References and Notes

(1) Tyndall, G. S.; Cox, R. A.; Granier, C.; Lesclaux, R.; Moortgat, G. K.; Pilling, M. J.; Ravishankara, A. R.; Wallington, T. J. *J. Geophys. Res.* **2001**, *106*, 157.

(2) Kesselmeier, J.; Staudt, M. *J. Atmos. Chem.* **1999**, *33*, 23.

(3) Jacob, D. J.; Heikes, B. G.; Fan, S. M.; Logan, J. A.; Mauzerall, D. L.; Bradshaw, J. D.; Singh, H. B.; Gregory, G. L.; Talbot; R. W.; Blake, D. R.; Sachse, G. W. *J. Geophys. Res.* **1996**, *101*, 24235.

(4) Herman, I.; Nguyen, T. L.; Jacobs, P. J.; Peeters, J. *J. Am. Chem. Soc.* **2004**, *126*, 9908.

(5) Soto, M. R.; Page, M. *J. Phys. Chem.* **1990**, *94*, 3242.

(6) Aloisio, S.; Francisco, J. S. *J. Phys. Chem. A* **2000**, *104*, 3211.

(7) Alvarez-Idaboy, J. R.; Mora-Diez, N.; Boyd, R. J.; Vivier-Bunge, A. *J. Am. Chem. Soc.* **2001**, *123*, 2018.

(8) Vanderberk, S.; Peeters, J. *J. Photochem. Photobiol., A* **2003**, *157*, 269.

(9) Vandenberk, S.; Vereecken, L.; Peeters, J. *Phys. Chem. Chem. Phys.* **2002**, *4*, 461.

(10) Masgrau, L.; Gonzalez-Lafont, A.; Lluch, J. M. *J. Phys. Chem. A* **2002**, *106*, 11760.

(11) Peeters, J.; Fantechi, G.; Vereecken, L. *J. Atmos. Chem.* **2004**, *48*, 59.

(12) Dransfield, T. J. Manuscript in preparation.

(13) Poggi, G.; Franscisco, J. S. *J. Chem. Phys.* **2004**, *120*, 5073.

(14) Singleton, D. L.; Paraskevopoulos, G.; Irwin, R. S. *J. Am. Chem. Soc.* **1989**, *111*, 5248.

(15) Butkovskaya, N. I.; Kukui, A.; Pouvesle, N.; Le Bras, G. *J. Phys. Chem A* **2004**, *108*, 7021.

(16) Dagaut, P.; Wallington, T. J.; Liu, R.; Kurylo, M. J. *Int. J. Chem. Kinet.* **1988**, *20*, 331.

(17) Sander, S. P.; Friedl, R. R.; Golden, D. M.; Kurylo, M. J.; Huie, R. E.; Orkin, V. L.; Moortgat, G. K.; Ravishankara, A. R.; Kolb, C. E.; Molina, M. J.; Finlayson-Pitts, B. J. *Chemical Kinetics and Photochemical Data for Use in Stratospheric Studies*, Evaluation No. 14, JPL Publication 02-25; JPL Pasadena, CA, 2003.

(18) Atkinson, R. A. *J. Phys. Chem. Ref. Data Suppl.* **1994**, *2*, 1.

(19) Smith, I. W. M.; Ravishankara, A. R. *J. Phys. Chem. A* **2002**, *106*, 4798.

(20) Peeters, J.; Vandenberk, S.; Piessens, E.; Pultau, V. *Chemosphere* **1999**, *38*, 1189.

(21) *Facsimile for Windows*, version 4.0; UES Software Inc.: Dorchester, U.K.

(22) Vandenberk, S.; Vereecken, L.; Peeters, J. *Phys. Chem. Chem. Phys.* **2002**, *4*, 461.

(23) DeMore, W. B.; Sander, S. P.; Golden, D. M.; Hampson, R. F.; Kurylo, M. J.; Howard, C. J.; Ravishankara, A. R.; Kolb, C. E.; Molina, M. J. *JPL Pub.* **1997**, *97-4*, 1.

(24) Deters, R.; Otting, M.; Wagner, H.; Laszlo, B.; Dobe, S.; Berces, T. *Ber. Bunsen−Ges.* **1998**, *102*, 58.

(25) Staker, W. S.; King, K. D.; Gütsche, G. J.; Lawrance, W. D. *J. Chem. Soc., Faraday Trans.* **1991**, *87*, 2421.

(26) Gütsche, G. J.; Lawrance, W. D.; Staker, W. S.; King, K. D. *J. Phys. Chem.* **1995**, *99*, 11867.

(27) Tsang, W.; Hampson, R. F. *J. Phys. Chem. Ref. Data* **1986**, *15*, 1.

(28) Baulch, D. L.; Cobos, C. J.; Cox, R. A.; Esser, C.; Frank, P.; Just, T.; Kerr, J. A.; Pilling, M. J.; Troe, J.; Walker, R. W.; Warnatz, J. *J. Phys. Chem. Ref. Data* **1992**, *21*, 411.

(29) Estimated at the G2M(CC,MP2) level of theory.

(30) Weast, R. C., Astle, M. J., Eds. *CRC Handbook of Chemistry and Physics*; CRC Press: Boca Raton, Fl.

(31) Frisch, M. J.; Trucks, G. W.; Schlegel, H. B.; Scuseria, G. E.; Robb, M. A.; Cheeseman, J. R.; Zakrzewski, V. G.; Montgomery, J. A. Jr.; Stratmann, R. E.; Burant, J. C.; Dapprich, S.; Millam, J. M.; Daniels, A. D.; Kudin, K. N.; Strain, M. C.; Farkas, O.; Tomasi, J.; Barone, V.; Cossi, M.; Cammi, R.; Mennucci, B.; Pomelli, C.; Adamo, C.; Clifford, S.; Ochterski, J.; Petersson, G. A.; Ayala, P. Y.; Cui, Q.; Morokuma, K.; Malick, D. K.; Rabuck, A. D.; Raghavachari, K.; Foresman, J. B.; Cioslowski, J.; Ortiz, J. V.; Baboul, A. G.; Stefanov, B. B.; Liu, G.; Liashenko, A.; Piskorz, P.; Komaromi, I.; Gomperts, R.; Martin, R. L.; Fox, D. J.; Keith, T.; Al-Laham, M. A.; Peng, C. Y.; Nanayakkara, A.; Challacombe, M.: Gill, P. M. W.; Johnson, B.; Chen, W.; Wong, M. W.; Andres, J. L.; Gonzalez, C.; Head-Gordon, M.; Replogle, E. S.; Pople, J. A. *Gaussian 98*, revision A.9; Gaussian, Inc.: Pittsburgh, PA, 1998.

(32) Holbrook, K.; Pilling, M.; Robertson, S. *Unimolecular Reactions*, 2nd ed.; Wiley: New York, 1996.

(33) Gilbert, R. *Theory of Unimolecular and Recombination Reactions*; Blackwell Scientific Publications: Oxford, U.K., 1990.

(34) Forst, W. *Theory of Unimolecular Reactions*; Academic Press: New York, 1973.

(35) Vereecken, L.; Huyberechts, G.; Peeters, J. *J. Chem. Phys.* **1997**, *106*, 6564.

(36) Laidler, K. J. *Theories of Chemical Reaction Rates*; McGraw-Hill: London, 1969.

(37) Benson, S. W. *The Foundations of Chemical Kinetics*; McGraw-Hill: New York, 1960.

(38) Steinfeld, J. I.; Fransisco, J. S.; Hase, W. L. *Chemical Kinetics and Dynamics*; Prentice-Hall: New York, 1989.

(39) Johnston, H. S.; Heiklen, J. *J. Phys. Chem.* **1962**, *66*, 532.

(40) Becke, A. D. *J. Chem. Phys.* **1992**, *97*, 9173.

(41) Lee, A.; Yang, W.; Parr, R. G. *Phys. Rev. B* **1988**, *37*, 785.

(42) Mebel, A. M.; Morokuma, K.; Lin, M. C. *J. Chem. Phys.* **1995**, *103*, 7414.

(43) Scott, A. P.; Radom, L. *J. Phys. Chem.* **1996**, *100*, 16502.

(44) Curtiss, L. A.; Raghavachari, K.; Redfern, P. C.; Rassolov, V.; Pople, J. A. *J. Chem. Phys.* **1998**, *109*, 7764.

(45) Maçôas, E. M. S.; Khriachtchev, L.; Pettersson, M.; Fausto, R.; Räsänen, M. *J. Chem. Phys.* **2004**, *121*, 1332.